Coupling between ferromagnetic and conduction-spin-resonance modes at a ferromagnetic–normal-metal interface

R. H. Silsbee,* A. Janossy,† and P. Monod
Laboratoire de Physique des Solides, Universite Paris-Sud, 91405, Orsay, France
(Received 1 November 1978)

The transmission-electron-spin resonance (TESR) is measured on copper foils with ferromagnetic films of permalloy, iron, and nickel deposited on one surface. The greatly enhanced TESR resulting from the presence of the ferromagnetic film is studied as a function of orientation of the magnetic field which tunes the relative resonance frequencies of the ferromagnetic resonance (FMR) mode and the pure-copper TESR modes over a wide range. A phenomenological theory is developed from appropriate Bloch equations for the copper and for the ferromagnetic film, coupled by the transport of magnetization by the diffusion of electrons across the interface between the two metals. This theory describes well a number of distinct features of the experimental results.

I. INTRODUCTION

This paper presents a systematic study of conduction-electron-spin resonance (CESR) in a metallic plate which is in intimate contact with a thin ferromagnetic film. As this particular experimental geometry, which we call a "sandwich" or "layer structure," is not usually considered in the classical experiments concerning electron-spin resonance in metals, we will first review the essential physical parameters involved in such studies in order to be able to appreciate the new problems associated with this geometry.

The basic description of the physics of conduction-electron-spin resonance in a metal is contained in the work of Dyson[1] following the experiments of Feher and Kip.[2] In his classical paper Dyson solves the two essential questions: (i) what are the eigenmodes for spin resonance and diffusion and (ii) how are these modes coupled to or excited by an external radio-frequency (rf) field?

Dyson's solution shows that for most cases a well-defined resonance line exists, if the spin lifetime is not too short. The intensity, defined as the integral of the resonance line, and the line shape depend critically on the geometry of the sample and on its purity. More precisely these two quantities are determined by the boundary conditions imposed by the diffusion of the electrons in the skin-depth region and throughout the sample. When these are properly taken into account it is possible to determine the exact field for resonance, the spin lifetime, and the diffusion coefficient for the electrons. These three parameters essentially characterize the resonance eigenmode and do not depend on the geometry used. In all cases Dyson considered the metal to be homogeneous, that is, he assumed all the properties of the medium to be uniform in space through the bulk metal. However a brief account of the modifications necessary for inhomogeneous (surface) spin relaxation was also derived.

A direct extension of Dyson's ideas has been made by Lewis and Carver[3] for the case of the sample transmission technique. Closely following Dyson's argument, they show how transmission-electron-spin resonance (TESR) is made possible through a plane slab of pure enough metal.[4] The conclusion of this work is that the same physical parameters are involved in the analysis of the experiment as in the more usual reflection one. A natural question arises from this type of investigation, considering that the weakness of the observed signals is due to the combination of weak Pauli susceptibility and smallness of the skin depth: is it possible to separate the factors responsible for the excitation of the spins from those responsible for their resonance?

An original extension of the study of metals by CESR was made in this direction by the investigation of inhomogeneous metallic media. This can be achieved in a simple way by plating a second metal onto the original metal sheet in such a way as to insure a good electrical contact across the sandwich interface. Such structures have been studied for ^{5}Al:Zn and ^{6,7,8}Cu:Li double layers. These have been interpreted tentatively in terms of surface relaxation[7,8] and also by proper averaging of the properties of the electrons in each layer.[6]

Another way to produce an inhomogeneous metallic medium has been to use ion implantation[9]—indeed at typical energies of 200 keV the mean stopping range, of for example ^{55}Mn in Cu, is 600 Å; thus for doses of the order of 10^{15} ions/cm^2 it is possible to achieve a very thin layer (thinner than the skin depth) in which the magnetic properties of the host metal are entirely governed by those of the im-

planted ions. In the simpler cases, the analysis has been done by Hurdequint[10] and Walker[11] and can be sketched in the following manner: the eigenmode for resonance of the conduction-electron spin is identical to that of a very dilute homogeneous alloy containing the same number of magnetic ions (except for the diffusion coefficient). However the response of that mode to rf excitation is that of the implanted layer which will be much more strongly coupled than the pure metal, due to the greatly enhanced susceptibility. This results mainly in an appreciable gain in signal intensity, together with a shift and linewidth increment, due to the coupling of the electrons spins to the ions.

The feasibility of experiments with layered metallic sandwiches in which the electrons sample the properties of both layers, together with the spectacular result obtained by the magnetic coupling of electrons to the implanted magnetic ions, leads directly to the investigation of a ferromagnetic sandwich, that is the response of a normal metal in good contact with a ferromagnetic film. However, in this case a number of new questions arise compared to the simpler previous cases. Indeed the previously mentioned studies of layered structures were such that the g factors of both systems could be very close and the coupling mechanism with the base metal was strong enough so that it would not play a role in the final interpretation, very much like the strong-coupling "bottle-neck" limit of the Hasegawa problem.[12] Among the new parameters that are bound to affect the behavior of the ferromagnetic-paramagnetic problem are the nature of the interfacial coupling and its strength. This problem is by no means a new one and has been investigated by different techniques, in particular by Hoffman[13] following earlier studies in Grenoble. Their conclusions together with other studies aimed primarily at understanding the description of coupled ferromagnetic films, was that in the case of two ferromagnetic layers in close contact one can determine an exchange interaction at the boundary whose value is of the same order of magnitude as that of the bulk ferromagnet. However, as soon as the two layers were separated by a complete paramagnetic film (for instance 30 Å of Au) this coupling vanishes, and no conclusion could be drawn concerning the ferromagnetic-paramagnetic interaction. We think that our method of investigation offers a much more appropriate tool for this type of "weak" coupling situation than the ferromagnetic resonance study by itself. As reported briefly by Janossy and Monod,[14] using the transmission technique on a sandwich structure of copper and permalloy, magnetic coupling has been demonstrated experimentally between the permalloy film and the conduction electrons in the copper. It is the purpose of this paper to investigate in greater detail the experimental evidence in this case. The main purpose of such a study is twofold: (i) to understand the controlling factors of this coupling and its effect on the TESR resonance; and (ii) to get a phenomenological description of the motion of the coupled magnetizations.

The presentation is as follows: In Sec. II a simplified model for the coupled equations of motion is derived making clear the approximations involved and the general properties of the model. Section III is the experimental description of our results, which are discussed in Sec. IV on the basis of a more elaborate model presented in the Appendix. A number of conclusions are summarized in Sec. V.

II. SIMPLIFIED MODEL

As described in Sec. III, the experiment consists of the measurement of the transmitted ESR signal for a variety of values of ϕ, the angle between the applied magnetic field and the normal to the double layer sandwich. For general values of ϕ, the effect of depolarizing fields in the ferromagnetic film is to give an internal field in the ferromagnet which is not parallel to the applied field H_a, and the equations of motion for the ferromagnetic resonance (FMR), and the coupling at the interface become rather complicated. To reproduce the full calculation here would obscure both the important physical ideas and the approximations which are involved. Therefore, this section is devoted, after some generally applicable discussion, to a calculation for a hypothetical case in which the applied field is normal to the sample ($\phi=0$) and of sufficient magnitude ($>4\pi M_0$) so that the magnetization in the ferromagnet is also aligned perpendicular to the sample. In the experiments discussed later this geometry is never realized, since, for the fields of interest near 3200 G, H_a is less than $4\pi M_0$. Nevertheless, a discussion of this example illustrates most of the important ideas.

The geometry for this discussion is defined in Fig. 1, with a circularly polarized microwave field of amplitude h incident upon the ferromagnetic layer of thickness f; and we ask for the resultant transverse magnetization developed near the free surface of the paramagnetic layer of thickness p. This is compared with the corresponding magnetization in the absence of the ferromagnetic layer, the conventional TESR geometry, since finally the experimental results are compared with the simple TESR results and the transmitted fields are simply proportional to the magnetization at the back surface. Although the calculations, and most of the experiments, were carried out with the microwave field incident upon the ferromagnetic side of the sample, one anticipates identical results for the predicted transmitted fields if the roles of the ferromagnetic and paramagnetic layers are reversed. This is indeed the substance of the reciprocity theorem discussed by Walker[11] and is in accord

with a few early experiments in which the sense of transmission was reversed.

In the following we shall give a phenomenological model describing the coupling between dynamic magnetizations of a ferromagnetic and paramagnetic layer. We note that recently a somewhat different approach was also suggested.[15]

The ferromagnetic film is phenomenologically modeled as a system of localized moments (d electrons) described by the ferromagnetic moment $\vec{M}$,

microwave field h	→ drives	FMR d electrons m	→ drives	s electrons of ferromagnet m_f	⇄ interfacial coupling	s electrons of paramagnet m_s

(1)

The first arrow is one way, since our interest focuses on behavior moderately far from the ferromagnet resonance (FMR) condition where the loading of the microwave cavity by the FMR is insignificant. The second reflects the large ratio of the d electron to s-electron magnetization within the ferromagnet, such that the presence of the s electrons has little influence upon the FMR. The interfacial coupling cannot be treated as small, and is indicated by a double arrow in the diagram.

The FMR of the d electrons is described by the Bloch equation

$$\frac{d\vec{M}}{dt} = \gamma_F(\vec{M}\times\vec{H}) - \frac{\vec{M}-\vec{M}_0}{T_F} \tag{2}$$

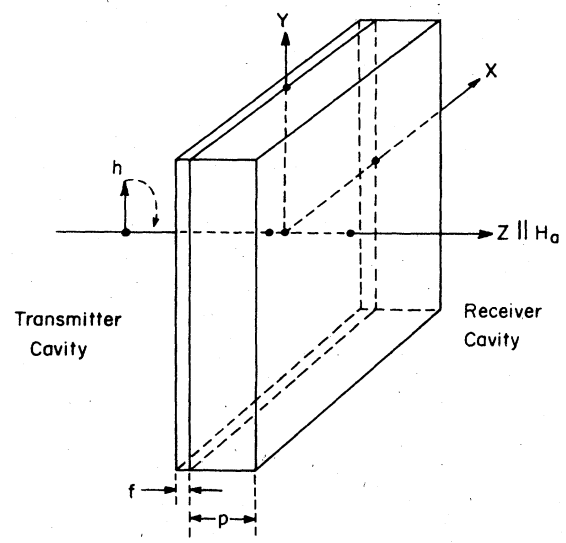

FIG. 1. Experimental geometry for simplified calculation.

coupled by exchange to itinerant (s electrons) which may diffuse across the interface between the ferromagnet and the paramagnet. This diffusion across the interface provides a mechanism coupling the magnetization of the two metals. A similar phenomenology may be constructed in which there are torques across the interface exerted by exchange forces. The experimental results show that this second model is inappropriate. The calculation proceeds as

with

$$\vec{H} = \hat{Z}H_F + (\hat{X}h_X + \hat{Y}h_Y) \ , \tag{3a}$$

$$\vec{M}_0 = M_0\vec{H}/|\vec{H}| \ . \tag{3b}$$

M_0 is the saturation magnetization of the film, and $H_F = H_a - 4\pi M_0$ is the internal field appropriate to the case of $\vec{H}_a$ normal to the foil. h_X and h_Y are the components of a circularly polarized microwave field which is assumed to be uniform over the thickness of the film. Only the uniform mode is treated here; the possible effects of spin waves are not considered. Denoting

$$M_X + iM_Y \equiv M^0 e^{-i\omega t} \ , \quad h_X + ih_Y \equiv he^{-i\omega t} \ , \tag{4}$$

the solution of Eq. (2) is of the usual form

$$M^0 = \frac{(i\gamma_F H_F + 1/T_F)hM_0/H_F}{i(\gamma_F H_F - \omega) + 1/T_F} \ . \tag{5}$$

Note that we have allowed the magnetization to relax towards the instantaneous field in Eq. (2), which assures that the solution (5) is appropriate in the limit $\omega \to 0$.

For the conduction electrons in the ferromagnetic film and the paramagnetic foil, we use the Bloch equation with diffusion,

$$\dot{\vec{m}}_i = \gamma_i(\vec{m}_i\times\vec{H}_i) - \frac{1}{T_i}(\vec{m}_i - \chi_i\vec{H}_i) + D_i\nabla^2(\vec{m}_i - \chi_i\vec{H}_i) \tag{6}$$

with $i = f$ or p for the ferromagnetic or paramagnetic layers respectively. Note that both the diffusion and relaxation terms are written in terms of deviations of m from the instantaneous and local equilibrium values as suggested by Torrey[16] and by Walker.[17] In the ferromagnetic film the conduction spins are

driven dominantly by the exchange interaction with the local moment magnetization $\vec{M}$, with the field $\vec{H}_f$ in Eq. (6) taken to be $\vec{H}_f = \lambda \vec{M}$. The corrections due to the presence of the applied dc and microwave fields are unimportant. In the paramagnet we take

$$\vec{H}_p = \hat{Z} H_a + (\hat{X} \cos\omega t - \hat{Y} \sin\omega t) h e^{-(1-i)Z/\delta} \quad . \tag{7}$$

In this treatment the skin depth is modeled as classical, although the experimental regime is in fact anomalous. The predicted phase of the transmitted signal will be somewhat in error, ~15 degrees, but the accuracy of the experimental results does not warrant a more detailed treatment. Defining

$$\delta \vec{m}_i \equiv \vec{m}_i - \chi_i \vec{H}_i \quad , \tag{8a}$$

$$\delta m_{iX} + i \delta m_{iY} \equiv \delta m_i \quad , \tag{8b}$$

Eq. (6) becomes, for the ferromagnet,

$$[i(\gamma_f \lambda M_0 - \omega) + (1/T_f - D_f \nabla^2)] \delta m_f = i \omega \chi_f \lambda M^0 \quad , \tag{9}$$

and for the paramagnet,

$$[i(\gamma_p H_a - \omega) + (1/T_p - D_p \nabla^2)] \delta m_p = i \omega \chi_p h e^{-(1-i)Z/\delta} \quad . \tag{10}$$

These equations are to be solved with the driving term for δm_f being the M^0 given by Eq. (5). They are subject to appropriate boundary conditions at the free surfaces, and at the interface between the foil and the film. Denoting the foil-film interface as $Z = 0$ and the thicknesses of the ferro- and paramagnetic layers by f and p, respectively, we take as boundary conditions at the vacuum interfaces

$$Z = -f: \ (\partial/\partial Z)(\delta m_f) = 0 \quad , \tag{11}$$

$$Z = p: \ (\partial/\partial Z)(\delta m_p) = 0 \quad . \tag{12}$$

Presuming no relaxation at these interfaces we require the normal component of the magnetization current, proportional to the gradient of the deviation of the magnetization from equilibrium, to be zero.

At the interface, $Z = 0$, we also presume no spin relaxation, allowing us to equate the magnetization currents on either side of the interface,

$$-D_p \frac{\partial}{\partial Z}(\delta m_p)|_{Z=0} = -D_f \frac{\partial}{\partial Z}(\delta m_f)|_{Z=0} \equiv J_m \quad , \tag{13}$$

neglecting small factors required if γ_f differs significantly from γ_p. Following ideas of Fredkin,[6,18] the magnetization flow across an interface between two paramagnetic metals may be expressed as

$$\vec{J} = \Gamma \left[\left(\frac{\vec{m}_A}{\chi_A} - \vec{H}_A \right) - \left(\frac{\vec{m}_B}{\chi_B} - \vec{H}_B \right) \right] \quad , \tag{14}$$

where $\vec{H}_A$ and $\vec{H}_B$ are the effective fields in the two metals, and Γ is a constant characteristic of the interface. This expression may be made plausible either on the basis of microscopic models for the interface, or by the following macroscopic argument. The magnetic part of the free-energy density for a weak paramagnet in magnetic field H is

$$\mathcal{F}_p = \tfrac{1}{2}(m^2/\chi_p) - \vec{m} \cdot \vec{H} \quad , \tag{15}$$

and the equilibrium condition $m = \chi_p H$ is the result of the requirement $\nabla_m \mathcal{F}_p = 0$, where ∇_m is the gradient with respect to the magnetization vector. In nonequilibrium situations we have $\nabla_m \mathcal{F}_p \neq 0$, and the magnitude of $\nabla_m \mathcal{F}_p$ is a measure of the departure of the system from equilibrium, giving the driving force for relaxation and transport processes. In the case of interfacial transport, Eq. (14) is the natural macroscopic prediction. Similarly, for nonequilibrium transport of magnetization in inhomogeneous media, one would predict magnetization currents to be

$$\vec{J}_m = -C \nabla (\nabla_m \mathcal{F}_p) = -C \nabla (\vec{m}/\chi_p - \vec{H}) \quad , \tag{16}$$

with C a phenomenological constant, and predict the diffusion term in the Bloch equation to be

$$-\nabla \cdot \vec{J}_m = \nabla \cdot [C \nabla (\vec{m}/\chi_p - \vec{H})] \quad . \tag{17}$$

This is just the form of the diffusion term in Eq. (6) in the homogeneous case, with C and χ_p independent of position. The boundary condition at $Z = 0$ then becomes Eq. (13) combined with

$$J_m = \Gamma(\delta m_f/\chi_f - \delta m_p/\chi_p) \quad . \tag{18}$$

We emphasize the importance of expressing the interfacial transport in terms of the deviation of m_f from its equilibrium value, i.e., $\delta m_f = m_f - \chi_f \lambda M$, rather than m_f itself. In most situations in magnetic resonance, the transverse magnetizations are large compared with the equilibrium magnetization in the instantaneous driving field, and the distinction between m and δm is not important. In this situation, however, where the driving frequency ω is very far from the s-electron resonant frequency $\gamma_f \lambda M_0$ in the exchange field of the d electrons we have $\delta m_f / m_f \sim \omega/\gamma_f \lambda M_0 \ll 1$ and the distinction is crucial. At first sight one might expect an *sd* bottlenecking to occur, making m_f precisely equal to $\chi_f \lambda M$, or $\delta m_f = 0$. The observation $\delta m_f \ll m_f$ is the observation that the system is indeed bottlenecked, but that the conduction electrons do not go to precise thermal equilibrium in the effective field λM.

This phenomenology does not define a microscopic mechanism for the interfacial coupling. The microscopic model adopted in this treatment is that of Janossy and Monod[5] and of Menard and Walker[19] and involves the transport of magnetization from one metal to the other by diffusion of electrons across the interface. In the crudest of such models the constant Γ is given by

$$\Gamma = v_F^f \chi_f t_f = v_F^p \chi_p t_p \quad , \tag{19}$$

where v_F^i, χ_i, and t_i are the Fermi-velocity, susceptibility, and -interfacial transmission coefficient for the conduction electrons on the $i(=p,f)$ side of the interface. The second of the equalities is assured by detailed balance arguments.

One could also imagine the transfer of magnetization across the interface by an exchange induced torque coupling from f to p at $Z=0$. The following phenomenology may also be used to describe this situation if Γ is replaced by an imaginary, rather than a real, constant characterizing this coupling.

Equations (9) and (10) with the boundary conditions (11)–(13) and (18) may be solved with the assumptions,

$$\delta m_f = A_f + B_f \cosh[k_f(Z+f)] \tag{20}$$

$$\delta m_p = A_p e^{-(1-i)Z/\delta} + B_p \cosh[k_p(Z-p)] \ , \tag{21}$$

which are chosen in part to satisfy the boundary conditions at $Z=-f,p$, under the experimental condition $\delta \ll p$. The algebra is straightforward but tedious, and the final answer is too cumbersome for simple interpretation. We note here some features of the solution and some reasonable physical approximations which allow a useful result to be obtained. The terms in $\cosh k_i Z$ in Eqs. (20) and (21) are solutions to the homogeneous part of Eqs. (9) and (10), and require

$$D_i k_i^2 = 1/T_i + i(\gamma_i H_{iZ} - \omega) \equiv \Omega_i \ , \quad i=f,p \ , \tag{22}$$

with

$$H_{pZ} = H_a \ , \tag{23}$$

$$H_{fZ} = \lambda M_0 \ . \tag{24}$$

k_f^{-1} and k_p^{-1} are the so-called spin depth in the film and the foil, the distance an electron will diffuse before undergoing a spin-relaxation process.[3] For these experiments the spin depth in the copper was larger than the foil thickness, and we use $pk_p < 1$ to allow

$$\sinh pk_p \to pk_p \ \text{ and } \cosh pk_p \to 1 \ . \tag{25}$$

In the ferromagnet on the other hand, the short mean free path in the evaporated film, together with the large value $i\gamma_f \lambda M_0$, of Ω_f in Eq. (22) for $i=f$, implies $fk_f > 1$ or

$$\cosh(fk_f), \ \sinh(fk_f) \to \tfrac{1}{2}\exp(fk_f) \ . \tag{26}$$

We also use

$$\lambda M_0 \gg \omega, 1/T_f \ . \tag{27}$$

Finally there appear three driving terms in the final solution. One of these, which becomes dominant only when the copper mean free path becomes shorter than the skin depth (classical skin-depth regime), has been omitted as unimportant. The amplitude B_p of the homogeneous solution in the ansatz Eq. (21) is the magnitude of the transverse magnetization at the copper vacuum interface, and is proportional to the signal transmitted through the foil. It becomes, with the approximations above,

$$B_p = \frac{\dfrac{(1-i)\omega\chi_p h\delta}{2p} + \dfrac{\Gamma\omega M^0}{p\gamma_f M_0}\left(\dfrac{D_f k_f}{D_f k_f + \Gamma/\chi_f}\right)}{\Omega_p + \dfrac{\Gamma}{p\chi_p}\left(\dfrac{D_f k_f}{D_f k_f + \Gamma/\chi_f}\right)} \ . \tag{28}$$

Note that the terms in the parentheses become equal to one as the coupling Γ becomes weak. These terms for Γ strong are the result of the influence of the interfacial coupling upon the ferromagnetic conduction-electron response δm_f, which in weak coupling is determined entirely through the driving via $\vec{M}$. In the following discussion these parentheses will be taken to be equal to one for simplicity.

With this simplification, and neglecting the damping term in the numerator of Eq. (5), Eqs. (5) and (28) become

$$\frac{M}{M_0} = \frac{i\gamma_F h}{i(\gamma_F H_F - \omega) + 1/T_F} \equiv \frac{i\gamma_F h}{\Omega_F} \tag{29}$$

and

$$B_p = ih\left(\frac{\gamma_F \Gamma\omega/\gamma_f p\,\Omega_f + (1+i)\omega\chi_p\delta/2p}{\Omega_p + \Gamma/p\chi_p}\right) \ . \tag{30}$$

These expressions illustrate a number of important features of the more complicated results obtained in the Appendix.

(a) The TESR signal will show a Lorentzian form determined by $1/(\Omega_p + \Gamma/p\chi_p)$, as long as the FMR is sufficiently detuned that the change in Ω_F is small as one sweeps through the TESR resonance.

(b) The amplitude and phase of the transmitted signal are determined by the sum of the coupling via the FMR and the direct coupling to the microwave fields, the two terms in the numerator of Eq. (30). If the FMR coupling dominates, there should be a change in phase and amplitude of the transmitted signal as the phase and amplitude of Ω_F^{-1} are altered by varying the orientation of the magnetic field.

(c) If the broadening of the TESR by the interfacial coupling $\Gamma/p\chi_p$ dominates over the bulk relaxation $1/\Gamma_p$, then the peak amplitude of the TESR becomes independent of the coupling strength, $B_{\text{peak}} = i\omega\chi_p h/\Omega_F$, but still reflects the FMR denominator.

(d) The result above was obtained under the assumption of coupling between the metals by transport of magnetization by the diffusive motion of electrons across the interface. One might alternatively have proposed an exchange coupling across the interface, the paramagnetic magnetization feeling a torque related to the ferromagnetic magnetization. Such a model leads to results essentially the same as the above,

with the simple replacement of Γ by an imaginary constant whose sign is determined by whether the interfacial coupling is ferromagnetic or antiferromagnetic. Again one predicts an enhancement, but now there is a different phase relative to the directly coupled signal, and, instead of a broadening of the signal, we have a shift proportional to Γ.

(e) Both the FMR coupled TESR, B_p, and the FMR, M, depend upon $1/\Omega_F$. Our characterization of the films is poor and we have neglected effects of anisotropy fields, so that we can not confidently predict Ω_F, particularly near $\phi=0$. However by measuring M experimentally we avoid these ambiguities and obtain a direct measure, within a proportionality constant, of Ω_F and are therefore able to make a quantitative comparison with the predicted $1/\Omega_F$ dependence of B_p.

For quantitative comparison of the results with the model, it is necessary to take into account a number of details, including the elliptical polarization of the FMR mode, and the fact that the macroscopic H field in the ferromagnet and in the paramagnet are not parallel. In the Appendix is an outline of the solution taking into account the appropriate polarizations, but with the physical approximations which led to Eq. (30) based on the numerical values deduced from the experiment.

III. EXPERIMENTAL METHOD AND RESULTS

The samples were all prepared by ultrahigh vacuum evaporation of the ferromagnetic layer onto a well-prepared surface of Cu. The copper used was in the form of single-crystal slices of $\frac{1}{2}$-in. diameter grown in a graphite crucible in vacuum from high-purity ASARCO 99.999% Cu; the residual resistivity ratio at 4.2 °K was typically 2000 and the limiting TESR full linewidth at low temperature was 20 G, for a copper foil without a ferromagnetic layer.

Prior to insertion into the evaporator, both surfaces were carefully chemically polished to remove damage from the spark cutting of the slices. The thicknesses of the final slices are given in Table I and range from 60 to 110 μ. Before evaporation and after the usual outgassing procedure of the evaporator, an anneal at 600 °C for 15 h in 10^{-8}-Torr vacuum was performed by heating the stainless-steel sample holder onto which the samples were mechanically clamped. This was done in order to eliminate possible contamination of the surface. (In the case of Cu-Permalloy 200 Å and Cu-Permalloy 1000 Å this procedure was followed at Bellevue by H. Pascard. For CuNi, CuFe, and Cu-Permalloy No. 1 the final heating was done at 370 °C for 10 h in 10^{-7}-Torr vacuum.) The evaporation was made by a 3 kw electron gun from a water-

TABLE I. Data summary.

Run	Sample	Relative Peak TESR Amplitude at $\phi=90°$	Full Linewidth (Gauss)	Foil Thickness (μm)	Γ'/χ_p (10^7 cm/sec)	Film Thickness from χ_F (Å)
Pure Copper, Standard Sample[a]		22	17	40		
1/31	1000-Å Py[b]	13	273	60	1.3	
3/20	1000-Å Py	10	230	60	1.1	
5/2	200-Å Py	12	268	70	1.5	
6/6, 6/14	Py #1	11	112	150	1.0	150,220
5/21, 6/25	Ni #1	3.7	143	60	0.6	150
5/23	Fe #1	1.1	138	63	0.6	
5/24	copper only	3.0	45	63		
5/28	Fe #2	1.8	134	63	0.6	150
5/30	after anneal	5.1	210	63	0.9	200
6/4	Fe #3	9.5	198	63	1.0	240

[a]Hurdequint, thesis.
[b]Py: Permalloy.

cooled crucible. For the 200- and 1000-Å Permalloy, this was deposited at a rate of 4 Å per second and 10^{-8}-Torr vacuum with the copper substrate at room temperature. For the CuNi, CuFe, and Cu-Permalloy No. 1 the deposition rate was about 3 Å sec^{-1} and was made on the copper substrate at 370 °C. No essential difference was noted in these differently deposited samples.

However on one occasion, on an early attempt to evaporate Fe on Cu, a vacuum of the order of 10^{-1} Torr was present by mistake during evaporation and enough contamination was produced on the copper to prevent the magnetic coupling to occur. Similar more systematic observations have been made by Hoffman.[13] The thickness was approximately given by a quartz frequency monitor, together with the rate of evaporation. No special precaution was taken once the samples were made other than to keep them under clean 10^{-6}-Torr vacuum when not in use. The samples were run many times at large (~6 months) intervals without showing any tendency of evolution.

The principal experimental results are the measurements of the position, peak intensity, line width, and phase of the TESR signal for a number of orientations of the applied field relative to the plane of the sample foil. Figure 2 gives a plot of γ_F^{-1} times the theoretical resonance frequencies [see Eqs. (A6) and (A7) for definitions] of the ferromagnetic resonance $(H_i H_k)^{1/2}$ as a function of the applied field orientation ϕ, for nickel, iron, and permalloy films at an applied field equal to the resonance field for the TESR in copper, namely, 3300 G at microwave frequency of 9200 ± 50 GHz, and assuming no anisotropy field. Noting that the resonance denominator Δ for the FMR is essentially $\gamma_F^2 H_i H_k - \omega^2$ one sees that there is wide range of variation of Δ available by varying ϕ from 90° with H_a parallel to the film, to 0° with H_a perpendicular to the film.

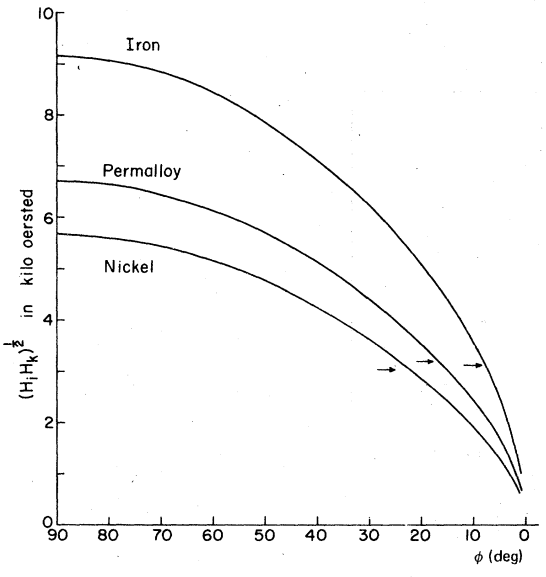

FIG. 2. Ferromagnetic resonance frequency divided by γ_F as a function of the angle of the applied magnetic field with respect to the normal to the film for a fixed magnitude of the applied field. Vertical position of the arrows is the applied microwave frequency divided by γ_F. The intersection of the arrows with the curves gives the magnet orientation for which the ferromagnetic and paramagnetic resonant frequencies are equal.

The TESR measurements are for the most part conventional. The temperature, typically between 20 and 30 °K, is chosen as high as possible to suppress transmission associated with cyclotron motion of the electrons. It is below the temperature at which the intensity of the resonance begins to be reduced by the spin-diffusion length becoming comparable with the thickness of the copper sample. The phase of the bias power to the receiver crystals was always adjusted to give line shapes of absorption symmetry. This phase setting was recorded with the data and is referred to as the phase of the transmitted signal. The TESR spectrometer is further provided with a "calibrated leak," a microwave path in parallel with the sample cavities, provided with variable attenuation and phase, such that meaningful phase and amplitude comparisons can be made between different runs. In this way it has been possible to compare the phase and amplitude of the enhanced FMR signal with the normal TESR signal of a simple copper sample.

In addition to the measurement of the TESR signals, a minor modification of the spectrometer allowed the measurement, in reflection, of the real and imaginary parts of the susceptibility χ_F' and χ_F'' of the FMR of the ferromagnetic film in the transmitter cavity. Similar measurements using the receiver cavity, exposed only to the copper side of the sample foil, indicated a measurable dependence of the cavity Q and resonant frequency upon the magnitude and orientation of the magnetic field. These variations, possibly due to magnetoresistance effects in the cavity walls or sample foil, were assumed to be the same in both the receiver and transmitter cavities, and were subtracted from the susceptibility data for the FMR as a background correction. Although unimportant near the FMR, the corrections amounted to 10 to 20% of the χ' for the magnet angles near the perpendicular and parallel orientations. Uncertainties in this correction represent a significant ambiguity in the quantitative comparisons discussed later. To verify semiquantitatively the interpretation of the FMR data, the fits to the absolute magnitude of the observed $\chi_F'(\omega)$ for the parallel configuration at fields well above the resonance field were used, along with a measurement of the transmitter cavity Q to calculate the thickness of the ferromagnetic film, assuming bulk values for the $4\pi M_0$ of the samples. Be-

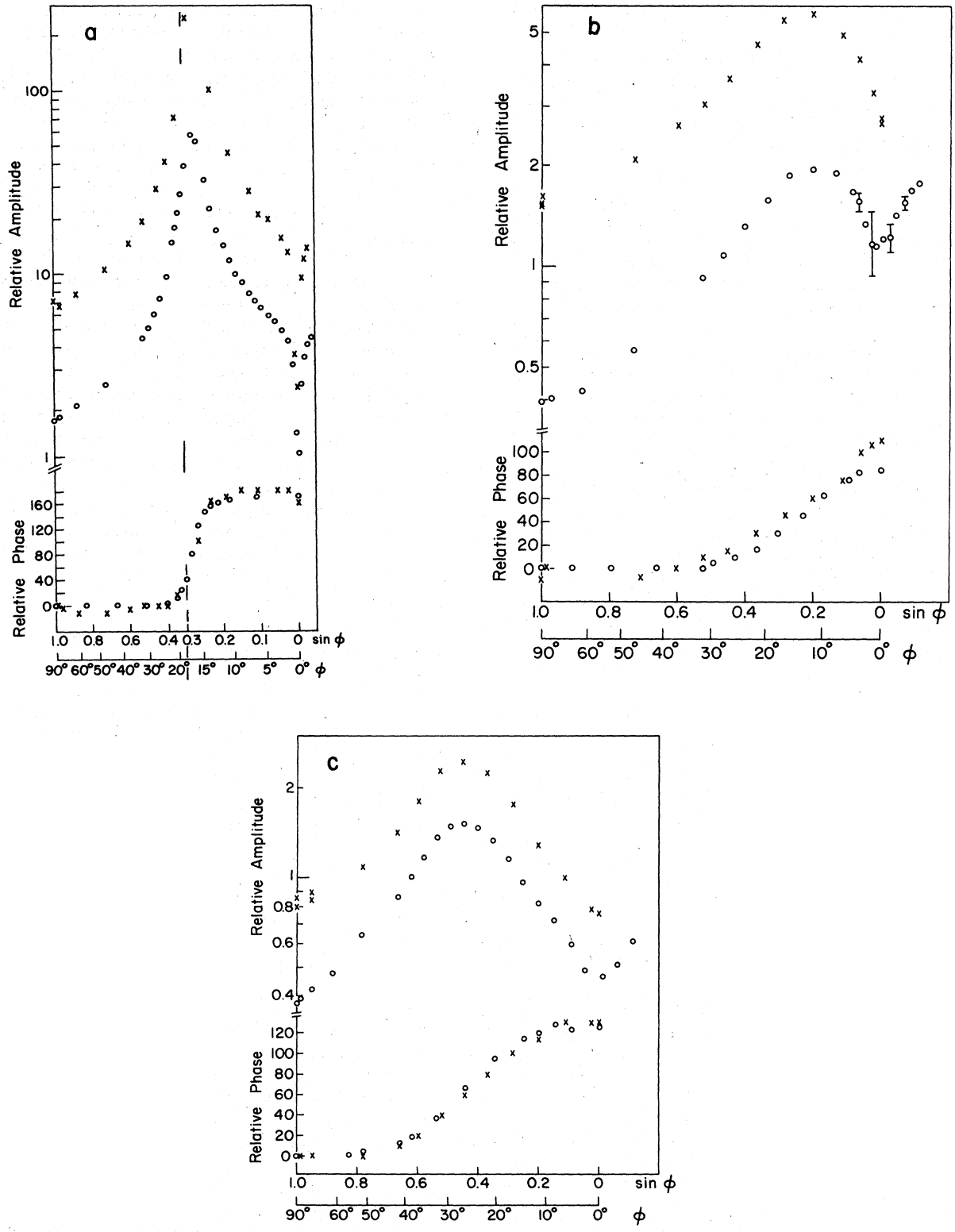

FIG. 3. Comparison of FMR and TESR results for (a) Permalloy, (b) Iron, (c) Nickel. ○, $|\chi_F|$ or $\tan^{-1}(\chi_F''/\chi_F')$ and ×, Amplitude or phase of TESR. The upper curves give the magnitude of χ_F and the TESR versus magnet orientation; the lower curves give the phase results. Note that the abscissa is linear in $\sin\phi$; in (a) there is a scale change at $\sin\phi = 0.3$.

cause of standing-wave problems in the microwave plumbing, the absolute signal intensities were accurate only to the order of ±50%, but the film thicknesses so deduced, see Table I, are in quite satisfactory agreement with the nominal value of 200 Å for all the films for which the comparison was made.

Figure 3 presents the results of the peak TESR signal and of the magnitude of the FMR susceptibility $\chi_F \equiv (\chi_F'^2 + \chi_F''^2)^{1/2}$ as a function of magnet orientation ϕ. The results shown for the TESR and χ near the "magic angle" at which $\omega_F = \omega_P$ are of doubtful quantitative significance because of substantial loading of the transmitter cavity by the FMR. In Fig. 3 are also given the phase of the TESR signal, to within an additive constant, as well as the phase of the FMR susceptibility, $\tan^{-1}(\chi_F''/\chi_F')$, again as the magnet angle is varied. Quite evident is the resonance in the susceptibility χ_F at the angles $(H_i H_k)^{1/2} = H_a$, as well as the striking correlation between TESR and FMR responses. For the nickel and iron samples, there is still appreciable χ'' at the perpendicular orientations suggesting either strong damping of the resonance or, more probably, the presence of anisotropy fields which can maintain a nonzero FMR frequency for perpendicular applied field.

Within a few degrees of the perpendicular orientation the TESR and FMR responses for the Permalloy sample show a very rapid variation with ϕ. This is the consequence of a slight sample misalignment from the vertical; as ϕ passes through zero the projection of H_a on the sample foil rotates rapidly from 0 through $\frac{1}{2}\pi$ to π. This interpretation is confirmed by the χ' of the same Permalloy sample at lower applied fields illustrated in Fig. 4. The linear variation of the dashed line is that predicted by Eq. (A19), for $\cos^2\gamma = 1$; the prediction of Eq. (A19) is that $\chi' \to 0$ for weak damping at $\phi = 0$, $\gamma = \frac{1}{2}\pi$ since $H_i = 0$ at $\phi = 0$, and indeed one sees a dramatic decrease or "notch" in χ' as one sweeps through $\phi = 0$.

A rough analysis of the results of Fig. 4 indicates, from the low-field data, a weak hysteresis near $\phi = 0$, the hysteretic shift at $H_a = 475$ and 950 oersted corresponding to a change in the component of H_a parallel to the film of about 20 oersted. This hysteretic shift is not measurable at the field of interest 3300 oersted though it probably contributes in part to the observed width of the notch at this field. The higher-field data, including roughly an estimate of the hysteretic effect, indicate a vertical sample misalignment ϵ of about $\frac{1}{2}$ degree.

Table I summarizes the intensities and line widths of the TESR for a number of runs with different samples. Additional important experimental results are the following:

(a) In none of the samples was the TESR displaced from that of a pure-copper sample by more than 3 G; the apparent g factor was 2.033 ± 0.005 in all cases measured. These measurements were made generally for the field parallel configuration, that is far from the peak enhancement; for angles near the peak enhancement some shift might be expected from the field dependence of Ω_F (or Δ).

(b) Line shapes were not measured carefully but appeared to be Lorentzian except near the angle of degeneracy of the TESR and FMR modes of Fig. 2, and at higher temperatures where the condition $pk_p \ll 1$ was not satisfied. In both cases extra lobes appeared in the wings of the lines which are qualitatively predicted by the theory but were not studied quantitatively.

(c) The line widths of the TESR signals were independent of magnet angle to within the precision of the experiment, typically ±5%.

(d) The phase of the TESR signal when enhanced by the ferromagnetic layer in the parallel geometry was equal to 110 ± 15° in advance of the phase for normal metal samples.

(e) An aluminum sample was also prepared with a Permalloy film, but with no attempt made to remove the oxide layer on the aluminum foil before evaporation of the ferromagnetic layer. The signals with and

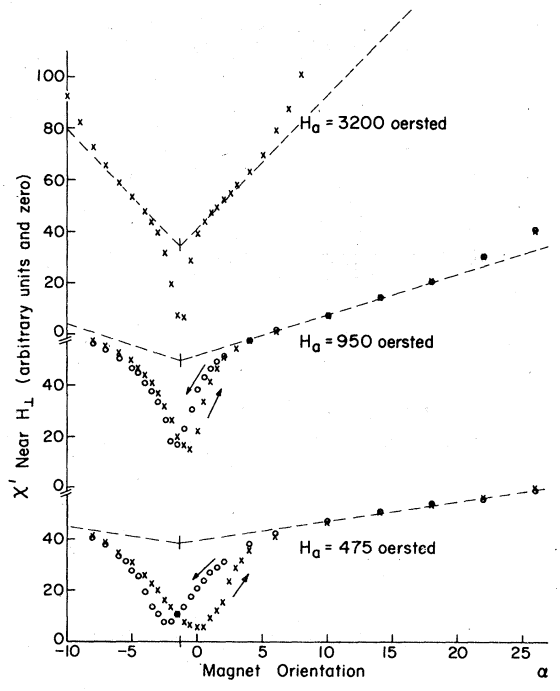

FIG. 4. FMR χ' as a function of field orientation for the field near normal for a Permalloy sample and at several fields. Evident are both the effects of the foil misalignment and hysteresis. At the field of interest, ~3200 oersted, the hysteretic effects are not important for Permalloy. Note that true value of $\phi = 0$ is at nominal $\phi = -1\frac{1}{2}°$.

without the ferromagnetic layer were the same. Similarly, copper samples with poorly prepared surfaces showed little or no enhancement with an added Permalloy film.

IV. DISCUSSION OF RESULTS

Because the Permalloy FMR showed a much narrower line width (~90 G at $\phi = 90°$) than the nickel or iron, it was the most extensively studied and the discussion will focus primarily on the Permalloy results. Again because of this narrow line width it is a good approximation to neglect the damping terms, involving $1/T_F$, in Eqs. (A19)–(A22) of the Appendix.

In the Appendix we have calculated both the susceptibility of the ferromagnetic film and the TESR response of the composite system as a function of the angles ϕ and γ defining the orientation of the applied dc magnetic field. ϕ is the angle of the applied field with respect to the horizontal projection of the normal to the nearly vertically oriented sample foil, and γ is the complement of the angle between the projection of the dc field onto the sample foil and the direction (~ vertical) of the microwave magnetic field. For ϕ greater than a few degrees, this projection is nearly perpendicular to the microwave field and $\gamma \simeq 0$; near the perpendicular field orientation the slight misalignment ($\sim\frac{1}{2}°$) of the foil results in a rotation of the projection through $\gamma = \frac{1}{2}\pi$ as ϕ goes through zero. In the expressions θ is the angle between the static-ferromagnetic magnetization and the normal to the foil, and $\theta_c = \cos^{-1}(H_a/4\pi M_0)$ defines the magnetization orientation for the case of a normal applied field of magnitude less than $4\pi M_0$. The results of the Appendix become, with the neglect of relaxation terms in the FMR,

$$\chi_F = \frac{\gamma_F M_0}{\Delta}(\gamma_F H_k \cos^2\gamma + \gamma_F H_i \cos^2\theta \sin^2\gamma) \ , \tag{31}$$

for $\gamma = 0$,

$$B_{p+} = \frac{h_1}{\Omega_p + \Gamma'/p\chi_p}\left[\frac{-(1+i)\omega\chi_p\delta}{2p} + \frac{i\Gamma'\omega\gamma_F}{p\Delta\gamma_f}\left(\omega + \gamma_F H_k \cos(\theta-\phi) + \frac{i\omega T_f}{1-i\omega T_f}\gamma_f 4\pi M_0 \sin\theta\cos\theta\sin(\theta-\phi)\right)\right] \ , \tag{32}$$

and for $\phi = 0$, $\gamma = \frac{1}{2}\pi$,

$$B_{p+} = \frac{h_1}{\Omega_p + \Gamma'/p\chi_p}\left[\frac{-(1+i)\omega\chi_p\delta}{2p} + \frac{i\Gamma'}{p}\left(\frac{\omega^2\gamma_f}{\Delta\gamma_f}\cos^2\theta_c + \frac{i\omega T_f}{1-i\omega T_f}\sin^2\theta_c\right)\right] \ . \tag{33}$$

In these expressions, H_i and H_k are related to the internal and demagnetization fields in the ferromagnetic by

$$H_i \equiv H_a\cos(\theta-\phi) - 4\pi M_0\cos^2\theta \underset{\phi\to\pi/2}{\to} H_a \underset{\phi\to 0}{\to} 0 \tag{34}$$

$$H_k \equiv H_i + 4\pi M_0\sin^2\theta \underset{\phi\to\pi/2}{\to} H_a + 4\pi M_0 \underset{\phi\to 0}{\to} 4\pi M_0\sin^2\theta_c \ . \tag{35}$$

Ω_p and Δ are resonance denominators for the uncoupled TESR and FMR resonances,

$$\Omega_p = i(\gamma_p H_a - \omega) + 1/T_p \tag{36}$$

$$\Delta = (\gamma_F^2 H_i H_k - \omega^2 + 1/T_F^2) - 2i\omega/T_F \ . \tag{37}$$

The effect of the back reaction of the paramagnetic (p) response back onto the ferromagnetic conduction-electron (f) response is accounted for by the modified Γ,

$$\Gamma' \equiv \Gamma[D_f k_f/(D_f k_f + \Gamma/\chi_f)] \ . \tag{38}$$

Note that these results have the same general form as those of the discussion of Sec. II. The TESR is driven both by the normal coupling to the microwave field in the skin depth and by the coupling (Γ or Γ') to the ferromagnetic conduction electrons. The strength of the coupling via the ferromagnetic film reflects the ferromagnetic resonance denominator Δ. In addition the TESR resonance is broadened as a consequence of the coupling to the ferromagnet.

Not evident in the discussion of Sec. II are the terms in Eqs. (32) and (33) involving the factor $f(T_f) \equiv i\omega T_f/(1 - i\omega T_f)$. These terms arise from the fact that there may exist oscillating components of both the applied microwave field and the demagnetization fields which are parallel to the ζ direction, the direction parallel to the static $\vec{M}$. If the ferromagnetic conduction spins relax slowly, $\omega T_f >> 1$, $m_{f\zeta}$ remains constant and there will be a non-equilibrium $m_{f\zeta}$ which will contribute to the injection of magnetization into the paramagnet. On the other hand, if we have $\omega T_f << 1$, the ζ component of m_f relaxes effectively instantaneously to the varying ζ component of the effective field and there will be no such contribution.

The experimental results for the Permalloy indicate that the second situation in fact prevails. Comment was already made in Sec. III on the "notch" which appears at $\phi = 0$. A similar notch appears in the TESR data as well, and it is the depth of the "notch" which gives some indication as to the magnitude of ωT_f. From Eqs. (32) and (33) one can calculate the ratio of the predicted signal at the bottom of the notch ($\phi = 0, \gamma = \frac{1}{2}\pi$) to the value extrapolated into $\phi = 0$ from the behavior outside the notch ($\phi = 0, \gamma = 0$). Neglecting the direct coupling term and letting $\gamma_f = \gamma_F$ gives

$$\frac{B_{p+}(\gamma = \pi/2)}{B_{p+}(\gamma = 0)} = \frac{\omega[\cos^2\theta_c - f(T_f)\sin^2\theta_c]}{\omega + \gamma_F H_k \cos\theta_c [1 + f(T_f)]} ,$$

$$\underset{T_f \to \infty}{\longrightarrow} 1$$

$$\underset{T_f \to 0}{\longrightarrow} \frac{\omega \cos^2\theta_c}{\omega + \gamma_F H_k \cos\theta_c} \underset{\text{Permalloy}}{\longrightarrow} 0.054 . \tag{39}$$

The case of slow-relaxation ($T_f \to \infty$) would imply no notch in the TESR data, the use of rapid relaxation ($T_f \to 0$), implies a notch nearly as deep as for the susceptibility data. The existence of the notch for the permalloy data implies that the relaxation of $m_{f\zeta}$ is rapid compared with the microwave period, and consequently $\delta m_{f\zeta}$ is small. Ambiguities due to baseline uncertainties and nonperfect flatness of the sample foil limit the strength of the bound on T_f, but the data do indicate

$$|f(T_f)| < 0.2$$

or that

$$1/T_f > 5\omega \sim 3 \times 10^{11}\,\text{sec}^{-1} . \tag{40}$$

The quality of the data for the nickel and iron samples do not warrant such an analysis. The rest of this discussion will assume $f(T_f) = 0$ for all of the samples.

It is interesting to note parenthetically that the analysis of the notch in the TESR data does help distinguish among models which are chosen to describe the behavior of the ferromagnet. We have also considered a rather simpler model for the ferromagnet, assuming only a single magnetization density M, rather than two densities, one associated with local moments and another with the conduction electrons. The formal results are essentially the same as presented above except that the condition equivalent to Eq. (40), implies a longitudinal relaxation rate for the ferromagnetic magnetization which is much more rapid than the transverse rate, a situation deemed unacceptable to most practitioners of magnetic resonance. It was to avoid this problem that we were led to the more complex model presented here.

The calculation in the Appendix assumes a coupling by electron transport of magnetization across the interface. As indicated earlier, similar results are obtained under the assumption of a coupling in which the magnetization in the paramagnet is driven by a torque proportional to the magnetization in the ferromagnet. In this case however, the coupling constant becomes imaginary, and in the denominator of Eqs. (32) and (33), the term in Γ' contributes a shift rather than a width to the observed TESR. Using the value of $\Gamma'/\chi_p \sim 10^7$ cm/sec deduced below from the strength of the enhancement, one would predict a shift of $\sim$100–200 G. The observed absence of a g shift to within a few Gauss implies that the model giving Γ' real is the more appropriate. This result is confirmed by the measurement of the phase of the FMR enhanced signal relative to that for a simple-metal sample which is predicted to be, for the parallel geometry $\phi = 90°$, a phase advance of 135° for the skin-depth model used in the calculation. There are two physical contributions to this predicted phase advance of 135°. In the simple-metal experiment there is a phase lag of 45° associated with the average phase of the h_1 in the skin depth relative to its value at the surface, which does not appear in the case of the signal coupled via the FMR since the ferromagnetic layer is thin compared with skin depth. Also, in the simple-metal experiments, the transverse magnetization is created by the torque exerted by h_1 on m_z, giving as injection a time derivative of the transverse magnetization perpendicular to h_1 and hence 90° out of phase, in fact a phase lag of 90°, with respect to the resonant rotating component of h_1. In contrast, for the FMR coupled TESR, the transverse magnetization injected at the interface is in phase with the FMR magnetization, which in turn, for the parallel configuration with $\omega_F > \omega$, is in phase with h_1 [$\chi_F'(\omega) > 0, \chi_F''(\omega) \sim 0$], giving no phase lag between the injected m and h_1. The sum of these effects gives the predicted phase advance of 135°. For the anomalous skin effect with a smaller retardation in the skin than for the normal skin effect, this predict-

ed phase advance is somewhat less, going to 120° in the extreme anomalous limit. The observed phase advance for Permalloy samples in the parallel configuration is $110 \pm 15°$ in satisfactory agreement with the prediction. The agreement, together with the absence of a measurable g shift, indicates that the FMR enhancement is dominated by a mechanism giving a real value of Γ, such as the electron transport mechanism proposed here.

The absence of enhancement for the aluminum sample, with an oxide layer at the interface, and the poor quality copper samples suggests the need for intimate electronic contact at the interface and that the coupling is not simply via electromagnetic fields at the interface. This observation is consistent with the proposed mechanism requiring the diffusion of conduction electrons across the interface.

Although we have assumed [Eq. (18)] Γ to be a scalar, more generally it would be represented as a tensor quantity. The implications of an anisotropy of the coupling constant Γ have not been studied in detail. There seems no reason *a priori* to expect that the interfacial transport of the components of magnetization parallel to the ferromagnetic magnetization, for example, should be the same as for the perpendicular components. A naive calculation indicates that if there were an extreme anisotropy, $\Gamma_{\zeta\zeta}=0, \Gamma_{\xi\xi}=\Gamma_{\eta\eta}=\Gamma$ for example, the observed TESR line width, which is dominated in these experiments by the term $\Gamma/p\chi_p$, should be reduced by a factor of nearly 2 in going from $\phi=90°$ to $\phi=0°$. The absence of observable line width variations to within $\pm 5\%$ indicates that any anisotropy in Γ is small, of the order of 10% or less.

The results illustrated in Fig. 3 indicate clearly the strong correlation, both of the amplitude and of the phase, of the enhanced TESR signal with the FMR response, as measured by $\chi_F(\omega)$. In all cases the gross behavior is determined simply by the angular dependence of the resonance denominator for the FMR Δ. A more severe test of the predictions is obtained by plotting the ratio of the observed TESR to $|\chi|$ since here, in the theoretical prediction, the denominator cancels, giving, with neglect of the "normal" coupling and of terms in $1/T_F$,

$$\frac{B_+(\text{peak})}{\chi_F} \sim \frac{\omega+\gamma_F H_k \cos(\theta-\phi)}{\gamma_F H_k}, \qquad (41)$$

for the case $\gamma=0$ representing the situation for most of the experimental data. This relation gives a specific prediction concerning both the amplitude and phase of the TESR signal relative to the FMR susceptibility, measured at the TESR resonance field as a function of angle. Note that in B_+ only the coupling via the FMR is included, since for the results discussed here it dominates heavily over the direct coupling term.

The experimental amplitude ratios are shown in Fig. 5 along with the result, Eq. (41). The neglect of the FMR damping in Eq. (41) is certainly valid for the Permalloy samples for which the line width for the resonance at $\phi=90°$ of 100 G implies $\omega/T_F \lesssim 0.015$ which is quite negligible in the present context. These plots are not of significance for angles near the peak enhancement, both because of the cavity loading noted earlier and because the analysis has not been extended to fit the observed non-Lorentzian line shapes observed near the "magic angle" resulting from the development of a bottleneck (strong coupling limit) when $\omega_F=\omega_p$. For the nickel and iron samples the theoretical model does not fit the susceptibility data satisfactorily. For the iron sample, and to lesser degree for the nickel, there remains substantial absorption (χ'') both at zero field for $\phi=90°$ and as ϕ goes to zero at $H=3300$ G, whereas the predicted resonance frequency in both cases is zero. The finite absorption cannot be satisfactorily explained by assuming a large damping since

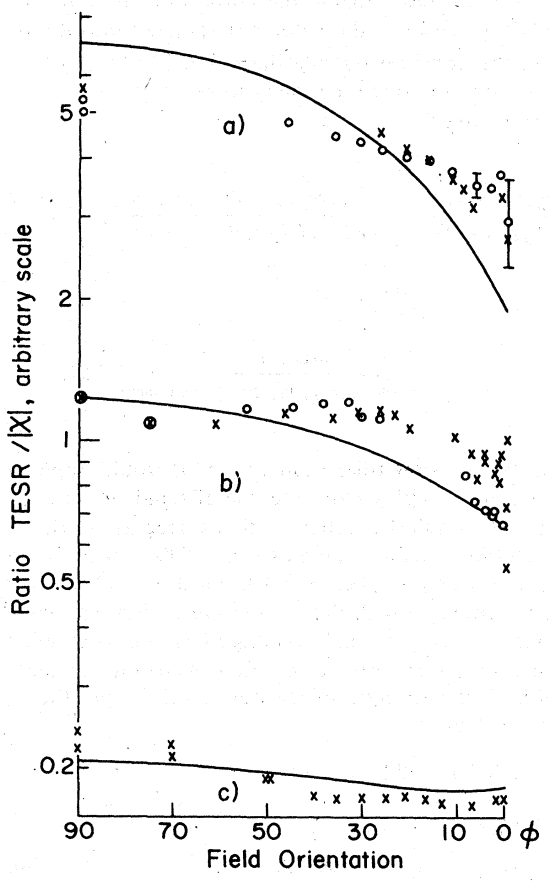

FIG. 5. Ratio of TESR peak amplitude to $|\chi_F|$ for (a) Iron, (b) Permalloy, (c) Nickel as a function of field orientation. ×, ○, experimental results; solid curve, the predictions of the theoretical model.

the χ'' data at $\phi = 90°$ do not show the long-high-field tail that would be predicted by a damping constant sufficient to give the observed χ'' at $H = 0$. It seems more likely that the very broad line in the iron and nickel is due to a distribution of anisotropy fields throughout the sample, giving a corresponding distribution of resonant fields. It should be noted that an anisotropy field of 400 G would be sufficient to displace the resonant field to zero for $\phi = 90°$ in the case of iron. For the case of iron ω/T_F is estimated to be $\lesssim 0.15$ and not of importance in the analysis. For nickel, ω/T_F may be as large as 0.5, in which case it begins to be an important correction to the ratio, but for the variation of B_+/χ_F with ϕ the effect is insignificant compared with the experimental uncertainties, both for the amplitude and the phase of B_+/χ_F. No attempt has been made to include the effect of anisotropy fields in the theory since the existing susceptibility data for the FMR are unlikely to be of sufficient precision to give a test at all critical of such a model. Rough arguments suggest that their inclusion would somewhat improve the agreement between experiment and theory for the iron.

The prediction of Eq. (41) is that the TESR phase and the phase of the ferromagnetic susceptibility χ_F, should show the same variation with magnet angle. Figure 3 illustrates that this prediction is well satisfied by the data. For the Permalloy samples, in which one sweeps fully through the resonance as ϕ is swept from 90° to 0°, the shift in phase is essentially 180° as noted by Janossy and Monod.[14] For the iron and nickel samples this phase shift is less complete, reflecting, in the present interpretation, nothing strange about the FMR-TESR coupling but simply complications associated with the FMR itself, perhaps the influence of anisotropy fields.

For the amplitude ratio, the agreement is less satisfactory, the predictions giving consistently a greater angular variation of B_+/χ_F than observed. These results are particularly sensitive to the background or apparent variation of the cavity χ with H and ϕ, alluded to earlier. The difference between the results for the two different Permalloy samples gives some indication of the lack of reproducibility. In addition, we have made no attempt to correct the results for the magnetic field inducted anisotropy of the diffusion constant for the electrons, D. Results on the angular variation of the TESR intensity for simple-copper samples indicate that, for the conditions of the runs for the double-layer samples, the angular variations due to anisotropy in D should be small, but perhaps not entirely negligible. Qualitatively one sees clearly both the decrease of B_+/χ_F as ϕ is varied from 90° to 0°, as well as the increase in magnitude of this variation in going from nickel to Permalloy to iron, both predictions of the diffusive coupling model. A more critical quantitative test will require better characterization of the FMR than was achieved in these experiments.

Perhaps the most striking prediction of the theoretical model is that within the limits of the model calculation, including the neglect of interfacial relaxation, the peak amplitude of the TESR signal is independent of Γ in the regime in which the coupling to the ferromagnet dominates the TESR line width. The model gives for this limiting peak-signal amplitude $B^0_{p+}(\Gamma)$ at $\phi = 90°$,

$$B^0_{p+}(\Gamma) = \chi_p h_1 \frac{\omega(\omega + \gamma_F H_k)}{\gamma_F^2 H_i H_k - \omega^2} \quad , \tag{42}$$

with the neglect of the FMR damping terms. This may be compared with the peak TESR signal for a simple-metal sample

$$B_{p+}(0) = \chi_p h_1 \frac{\delta\omega}{(2)^{1/2} p\,(1/T_p)} \tag{43}$$

to give

$$B^0_{p+}(\Gamma)/B_{p+}(0) = \frac{(\omega + \gamma_F H_k)(1/T_p)}{\gamma_F^2 H_i H_k - \omega^2} \frac{(2)^{1/2} p}{\delta} \quad , \tag{44}$$

where $1/T_p$ and p are the half-width of the TESR and the thickness for the simple-metal experiment.

Experimentally there is an indication of such a limiting peak amplitude. Three Permalloy samples (see Table I) give the same peak amplitude to within ±20%, despite substantial differences in the thickness either of the paramagnetic or ferromagnetic layers. This behavior is not observed, however, for the iron. Sample 1 showed essentially no FMR enhancement of the integrated area under the resonance, though a very substantial broadening when compared with the same sample foil in pure TESR after the iron was stripped off. This implies that there was substantial relaxation associated with the interface but no significant transfer of magnetization from the iron to the copper. Although the calculation neglects interfacial relaxation, the generalization is straightforward and requires the addition of a term Γ_r to Γ' in the resonance denominator (but *not* numerator) of the TESR in Eqs. (32) and (33). For this sample Γ_r was apparently large but Γ' was too small to give measurable coupling. A second iron sample showed weak enhancement of the area under the resonance and substantial breadth; an anneal resulted in a factor of 3 increase in the enhancement, and a factor of 2 increase in the excess breadth over the 45 G of the stripped sample. Thus the anneal is modifying the interfacial contact in such a way as to increase the efficiency of magnetization transport. Iron No. 3 prepared at a higher temperature shows even more enhancement. There are not enough data, however, to determine whether there is a saturation enhancement for the Fe. On the other hand, the enhancement for the iron No. 3 may be compared with the Permalloy results by correcting for the factors

$(\omega+\gamma_F H_k)/(\gamma_F^2 H_i H_k-\omega^2)$. The amplitude thus normalized is the same as for the Permalloy, indicating that the transfer Γ', dominates the relaxation Γ, or at least that Γ/Γ' is the same for the iron and Permalloy. For the single nickel sample, the normalized enhancement remains less by a factor of 3 than the Permalloy despite a strong coupling as indicated by the line width of the TESR; this seems to be a sample with the interfacial relaxation playing an important role.

A further test of this proposed limiting enhancement is the absolute value of the limiting enhancement, Eq. (44), in which appear only the resonance fields H_i and H_k for the FMR, and the remaining factors $1/T_p$, p, and δ referring to a reference sample without FMR enhancement. Using values for the stripped copper sample, which are consistent to within ±50% with those obtained by Hurdequint[10] on other copper samples, and using $\delta_A=0.14$ μm for the anomalous skin depth in copper, gives the prediction for Permalloy $B_{p+}^0(\Gamma)/B_{p+}^0(0)=6.8$, compared with the experimental result of 3.8 ± 1. This rough agreement in magnitude is convincing evidence that at the ferromagnet-paramagnet interface the magnetization transport is comparable with or dominant over the relaxation.

Finally the results may be interpreted to give numerical values of the interfacial transport coefficients Γ' under the assumption, verified roughly above, that interfacial relaxation is unimportant for the Permalloy and iron No. 3. The values of Γ'/χ_p listed in Table I are obtained from the line widths assuming a $1/T_p$ for the sample in absence of interfacial coupling of $\sim 4\times10^8$ sec^{-1} (full line width of 40 G), and in general represent the sum of broadening due to both transport and relaxation at the interface; for Permalloy and iron No. 3 they are dominated by the transport contribution.

In the theoretical model for the coupled systems, the rate of transfer of magnetization across the interface was described by a phenomenological constant Γ. This Γ is related to the Γ', deduced from the experimental results, by expression (A13). Since crude estimates indicated we have $D_f k_f \gtrsim \Gamma/\chi_f$ or that $\Gamma \gtrsim \Gamma'$, it is assumed here that $\Gamma=\Gamma'$. For an interface between two paramagnetic metals, one may obtain expressions for Γ in terms of simple models as discussed by Walker.[19] For such an interface, detailed balance requirements give conditions on the transmission and reflection coefficients as seen from the two sides of the interface. For models using spherical Fermi surfaces one has the reciprocity condition

$$v_{FA}\chi_A t_A = v_{Fb}\chi_B t_B \ , \tag{45}$$

where v_{Fi}, χ_i, and t_i are for metal i, respectively, the Fermi velocity, susceptibility, and an average over the Fermi surface of the interfacial transmission coefficient for electrons approaching from the side i. As a consequence, only in special cases will the transmission coefficient from the two sides be the same, as assumed by Walker,[19] and some modifications of his results are necessary as a consequence. Walker's arguments, with this generalization, lead to the result

$$\Gamma=\frac{v_F\chi t}{4}\frac{1}{1-\frac{1}{2}(t_A+t_B)} \ , \tag{46}$$

where v_F, χ, and t may, as a consequence of the relations (45), be that of either metal.

For the case of the contact between a ferromagnetic and a paramagnetic metal, it is by no means clear what to take for a microscopic model of the ferromagnet. It is tempting to avoid the issue, and we succumb to that temptation, by using the result Eq. (46) to estimate Γ, using values of v_F and χ appropriate to copper, letting $t_p=t_f$, and determining the value of this transmission coefficient which affords a fit to the Γ determined from the experiment. Note that the prediction is roughly $\Gamma/\chi_p \sim v_{Fp}$ the Fermi velocity in the paramagnet, if t is neither very small nor very near unity, reflecting crudely the idea that the Fermi velocity determines the rate at which magnetization can be delivered across the interface from one metal to the other. Assuming $t_f=t_p$, the data imply an interfacial transmission coefficient of $t\sim0.25$ for the Permalloy-copper interface representing quite a good contact between the two metals. Clearly many more experiments are required to determine whether this result is characteristic of the ideal contact between these metals or simply the accidental result for these particular samples.

V. CONCLUSIONS

Quantitative experiments have been carried out to characterize the enhancement of TESR signals provided by coupling to the TESR mode via a ferromagnetic film on one side of the TESR sample foil, and to elucidate the mechanism of this enhancement. The mechanism considered involves the coupling of the FMR mode in the film to the TESR mode in the foil by the diffusion of conduction electrons, polarized by the exchange field in the ferromagnet, into the paramagnetic foil providing an injection of transverse magnetization far in excess of that produced by the microwave magnetic field acting upon the equilibrium Pauli paramagnetic moment of the foil.

The experiments show unequivocally, through the scaling of the TESR enhancement with the ferromagnetic response in amplitude and phase, that the enhancement does involve the FMR mode of the film and that the mechanism is the same for the iron,

nickel, and Permalloy films. They, in addition, rule out mechanisms involving the coupling via torques exerted across the interface by exchange fields, since this mechanism would lead to a different phase of the transmitted signal from that observed and to a dramatic shift of the resonance, also unobserved.

The detailed phenomenological model developed in the Appendix accounts roughly for the angular variation of the ratio of the TESR to FMR response, though the deviations from the predictions do seem to be outside the experimental uncertainties and require further investigation. A most remarkable feature of the theory is that it predicts the absolute magnitude of the enhancement to be independent of the detailed properties of the ferromagnet, except its $4\pi M_0$, which determines the FMR frequency, and the magnitude of the coupling parameter Γ, as long as the appropriate inequalities are satisfied to validate the theory and provided that relaxation at the interface is negligible. The observed enhancement factor is within a factor of 2 of the predicted, and the discrepancy may well be associated with uncertainty in the skin depth of the copper, some reduction of the enhanced TESR due to the spin depth not being large compared with the sample thickness, or the presence of some interfacial spin relaxation. The broadening of the TESR by the interfacial coupling gives an estimate of Γ which indicates a probability of electron transmission through the interface from the copper to the films of about 25%. The absence of coupling in the case of the aluminum sample, with an oxide film at the interface, emphasizes the importance of intimate electronic contact at the interface, and eliminates coupling via interfacial electromagnetic fields as a mechanism for the observed enhancement.

We conclude that the proposed model, involving magnetization transport by the diffusion of conduction electrons across the interface, is in good accord with the experimental results.

ACKNOWLEDGMENTS

This work was largely carried out at the Laboratoire de Physique des Solides at Orsay, France, with the support of the Centre National de la Recherche Scientifique. One of the authors (R.H.S.) would like to thank the J. S. Guggenheim Foundation for the support which gave him the opportunity to work on this project. The work has also been supported by the NSF under the Grant No. DMR-77-08464, and via the Materials Science Center under the Grant No. DMR-76-81083, technical Report No. 3060.

APPENDIX

For the geometry and applied field strength, $H_a < 4\pi M$, used in these experiments the macroscopic field in the ferromagnetic film is not in general parallel to the applied field. As a consequence the Bloch equations for the FMR and for the δm_f resonance are conveniently written in one coordinate frame, while those for δm_p are conveniently written in a second. The boundary conditions at the interface then become complicated because of the need to project from one coordinate frame to the other. An additional complication is that the ferromagnetic resonance is now elliptically rather that circularly polarized. As in the main text, we take the paramagnetic foil to be thin and the ferromagnetic film to be thick compared with the respective spin depths, and ignore the additional driving term which becomes effective only as one enters the classical skin-depth regime. Figure 6 defines the coordinate frames used for the Bloch equations for $\bar{\mathbf{M}}$, δm_f, and δm_p. The axes X, Y, and Z are defined by the sample foil and microwave field geometry, with Z nearly horizontal and normal to the plane of the foil, X in the plane of the foil and horizontal, and Y nearly vertical in the plane of the foil and parallel to the microwave magnetic field. The x,y,z axes are defined by the applied magnetic field, and hence the field in the paramagnetic metal, with z parallel to the field, which is horizontal and rotatable about a vertical axis, and with x and y perpendicular to the field and, respectively horizontal and vertical. The axes Y and y are not quite parallel in the experiment as a consequence of a small misalignment, less than a degree, of the plane of the foil with respect to the vertical. For the paramagnetic metal this misalignment is of no consequence and Y will be taken to be parallel to y. The orientation of the field in the horizontal plane will be defined by $\phi = \sin^{-1}\hat{z}\cdot\hat{X}$. In the ferromagnet, the axes ξ, η, and ζ are defined as follows: ζ is parallel to the static magnetization and makes an angle θ with respect to Z; η is perpendicular to ζ, lies in the plane of the foil, and makes the angle γ with respect to Y; and ξ is perpendicular to ζ and η. For the ferromagnet, the small misalignment of the foil sample with respect to the axis of rotation of the applied field (H_a) is very important near $\phi = 0$. Since in these experiments H_a remains less than $4\pi M$ (M is the magnetization of the ferromagnet), in the geometry with $\epsilon = 0$, $\phi = 0$, M makes an angle $\theta_c = \cos^{-1}(H_a/4\pi M)$ with respect to the normal of the foil, but can lie anywhere on the cone defined by this angle. If the H_a is nearly, but not quite, normal, this degeneracy is lifted and the projection of M on the plane of the sample foil will be parallel to the projection of H_a on this same plane. With a slight misalignment of the foil from the vertical, as ϕ is swept from positive to negative values, the projection of H_a becomes parallel to Y, and hence γ becomes 90°, at $\phi = 0$, while for ϕ large compared with the misalignment, M remains essentially horizontal and γ remains near zero. Because the coupling between the microwave field and the magnetization M depends upon this angle γ, both the FMR

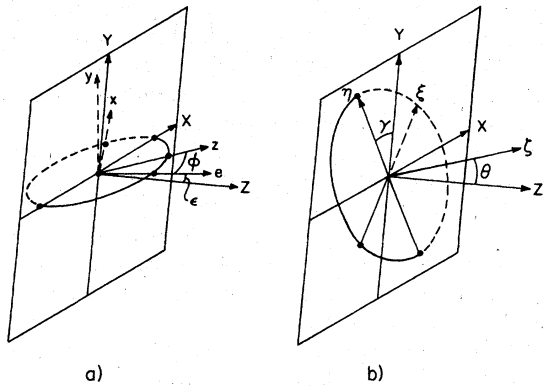

FIG. 6. Experimental geometry for the real experiment, i.e., (a) sample and TESR reference frames. X-Y, plane of sample; Z, normal to sample; y, vertical, normal to plane (circle) in which H_a rotates; e, intersection of Y-Z plane with plane of rotation of H_a; z, direction of applied field, H_a; x, normal to y and z; $\phi \sphericalangle e,z$, orientation of field; $\epsilon \sphericalangle e,Z = \sphericalangle y,Y$, foil misorientation; $\vec{h}_1$ is parallel to Y. (b) sample and FMR reference frames. X-Y, plane of sample; Z, normal to sample; ζ, direction of equilibrium ferromagnetic magnetization; η, intersection of the plane normal to ζ (circle) with X-Y; ξ, normal to η and ζ; θ, $\sphericalangle Z,\zeta$; γ, $\sphericalangle \eta, Y = \sphericalangle X$, (projection of ζ on foil) $= \sphericalangle X$, (projection of z on foil) $= \tan^{-1}(\epsilon \cot\phi)$ if $\epsilon << 1$.

coupled TESR signal and the FMR susceptibility vary quite rapidly near $\phi = 0$.

The angle θ is determined by the solution to the magnetostatic problem. For zero misalignment $\epsilon = 0$, this is obtained from the equations for the continuity of the appropriate components of B and H, and the assumption of zero anisotropy which implies that the magnetization M is parallel to the internal field H_i, i.e.,

$$H_a \sin\phi = H_i \sin\theta \ , \tag{A1}$$

$$H_a \cos\phi = (H_i + 4\pi M_0)\cos\theta \ . \tag{A2}$$

θ is then the solution of the transcendental equation,

$$H_a \sin(\phi - \theta) = 4\pi M_0 \sin\theta\cos\theta \ . \tag{A3}$$

In the (ξ, η, ζ) frame defined by the magnetostatic solution, with ζ making the angle θ with respect to the film normal, the Bloch equations for the FMR become

$$\dot{M}_\xi = \gamma_F H_i M_\eta - \gamma_F M_0 h_1 e^{-i\omega t}\cos\gamma - \frac{1}{T_F}\left[M_\xi - \frac{M_0}{H_k} h_1 e^{-i\omega t}\sin\gamma\cos\theta\right] \ , \tag{A4}$$

$$\dot{M}_\eta = -\gamma_F H_k M_\xi + \gamma_F M_0 h_1 e^{-i\omega t}\sin\gamma\cos\theta - \frac{1}{T_F}\left[M_\eta - \frac{M_0}{H_i} h_1 e^{-i\omega t}\cos\gamma\right] \ , \tag{A5}$$

with

$$H_i \equiv H_a\cos(\theta - \phi) - 4\pi M_0 \cos^2\theta \ , \tag{A6}$$

$$H_k \equiv H_i + 4\pi M_0 \sin^2\theta \ . \tag{A7}$$

The fields H_i and H_k, by including the effect of the demagnetizing fields produced by small deviations of M from its equilibrium position, represent the restoring torques resulting from deviations of M in the (η, ζ) and (ξ, ζ) planes, respectively. Denoting by M_ξ^0 and M_η^0 the amplitude of the transverse components of the driven FMR, the solutions of the Bloch equations are

$$M_\xi^0 = \frac{\gamma_F M_0 h_1}{\Delta}\left[i\omega\cos\gamma + \left(\gamma_F H_i + \frac{1}{\gamma_F H_k T_F^2} - \frac{i\omega}{\gamma_F H_k T_F}\right)\sin\gamma\cos\theta\right] \tag{A8}$$

$$M_\eta^0 = \frac{\gamma_F M_0 h_1}{\Delta}\left[\left(\gamma_F H_k + \frac{1}{\gamma_F H_i T_F^2} - \frac{i\omega}{\gamma_F H_i T_F}\right) \times \cos\gamma - i\omega\sin\gamma\cos\theta\right] \ , \tag{A9}$$

with

$$\Delta \equiv \left[\gamma_F^2 H_i H_k + \frac{1}{T_F^2} - \omega^2\right] - \frac{2i\omega}{T_F} \ . \tag{A10}$$

To simplify the resulting algebra we make from the outset the approximations noted in the main text, namely, in paramagnet,

$$k_p \delta_p << 1 \ , \quad \text{mean free path} > \delta \ , \quad k_p p << 1 \ , \tag{A11}$$

and in ferromagnet,

$$\omega, 1/T_F << \gamma_f \lambda M_0 \ , \quad k_f f >> 1 \ , \quad D_f k_f >> \Gamma/\chi_f \ . \tag{A12}$$

The last assumption is not satisfied, but greatly simplifies the algebra, since it allows the neglect of the influence of the interfacial magnetization transport on the conduction spin response in the ferromagnet, the left directed arrow in the scheme Eq. (1). Detailed calculation shows that the replacement of Γ by

$$\Gamma' \equiv \Gamma\left(\frac{D_f k_f}{D_f k_f + \Gamma/\chi_f}\right) \ , \tag{A13}$$

in the final result appropriately accounts for the error introduced by that assumption. [See the discussion after Eq. (28).]

The Bloch equations are now written for the ferromagnetic conduction electrons, keeping only the exchange field produced by the local-moment magnetization as the driving term for the transverse (ξ, η) components of δm_f as is consistent with the first of the inequalities (A12). For the ζ component it is essential to keep account of the driving microwave field h_1 and the oscillating demagnetizing fields as well.

$$\delta m_{f\xi}^0 \approx (i\omega\chi_f/\gamma_f M_0) M_\eta^0 \ , \tag{A14}$$

$$\delta m_{f\eta}^0 \approx (-i\omega\chi_f/\gamma_f M_0) M_\xi^0 \ , \tag{A15}$$

$$\delta m_{f\zeta}^0 = \frac{i\omega T_f \chi_f \sin\theta}{1-i\omega T_f}(h_1 \sin\gamma + 4\pi M_\xi^0 \cos\theta) \ . \tag{A16}$$

Note that these deviations are *not* zero in the strong bottleneck limit, and in fact do not depend upon the exchange-coupling parameter λ as long as it is large. Note also that even in first order in h_1 there is a nonzero $\delta m_{f\zeta}$. This is because there will be a component of h_1 parallel to ζ and also a component of the time-varying demagnetizing field parallel to ζ.

The calculation proceeds as in the text, the additional complication in obtaining the microwave ferromagnetic susceptibility as measured in the transmitter cavity,

$$\chi_F \equiv M_Y/h_1 \ , \tag{A17}$$

and the TESR response

$$B_{p+} \equiv (\delta m_{px} + i\delta m_{py})_{z=p} \ , \tag{A18}$$

being the need to project the $\vec{M}^0$ and $\delta\vec{m}_f^0$ as calculated in the ξ, η, ζ frame, into the (x,y,z) frame. One obtains, in the limiting cases,

for $\gamma = 0$

$$\chi_F = \frac{\gamma_F M_0}{\Delta}\left(\gamma_F H_k + \frac{1}{\gamma_F H_i T_F^2} - \frac{i\omega}{\gamma_F H_i T_F}\right) \ , \tag{A19}$$

$$B_{p+} = \frac{h_1}{\Omega_p + \Gamma/p\chi_p}\left\{\frac{-(1+i)\omega\chi_p\delta}{2p} + \frac{\Gamma}{p}\frac{\gamma_F}{\gamma_f}\frac{i\omega}{\Delta}\left[\left(\gamma_F H_k + \frac{1}{\gamma_F H_i T_F^2} - \frac{i\omega}{\gamma_F H_i T_F}\right)\cos(\theta-\phi) + \omega + \frac{i\omega T_f}{1-i\omega T_f} 4\pi\gamma_f M_0 \sin\theta\cos\theta\sin(\theta-\phi)\right]\right\} \tag{A20}$$

for $\gamma = \frac{1}{2}\pi$, $\phi = 0$,

$$\chi_F = \frac{\gamma_F M_0}{\Delta}\left(\frac{1}{\gamma_F H_k T_F^2} - \frac{i\omega}{\gamma_F H_k T_f}\right)\cos^2\theta_c \ , \tag{A21}$$

$$B_{p+} = \frac{h_1}{\Omega_p + \Gamma/p\chi_p}\left[\frac{-(1+i)\omega\chi_p\delta}{2p} + \frac{\Gamma}{p}\left(\frac{i\omega^2\gamma_F}{\Delta\gamma_f}\cos^2\theta_c - \frac{\omega T_f}{1-i\omega T_f}\sin^2\theta_c\right) + \left(\frac{1}{\gamma_F H_k T_F^2} - \frac{i\omega}{\gamma_F H_k T_F}\right) \times \frac{\Gamma}{p}\cos\theta_c\left(\frac{i\omega\gamma_F}{\Delta\gamma_f}\frac{\sin^2\theta_c\cos\theta_c 4\pi M_0\gamma_F}{\Delta}\right)\right] \ . \tag{A22}$$

As noted earlier, in these expressions the replacement Eq. (A13) generalizes the results to include the case $D_f k_f \lesssim \Gamma/\chi_f$. As in the earlier example discussed in the text, the TESR response B_{p+} and the ferromagnetic resonance both reflect the FMR resonance denominator Δ.

*Permanent address: Laboratory of Atomic and Solid-State Phys., Cornell Univ., Ithaca, N. Y. 14853.
†Permanent address: Central Research Institute for Phys. H-1525, Budapest, 114 P.O.B. 49, Hungary.

[1]F. J. Dyson, Phys. Rev. 98, 349 (1955).
[2]G. Feher and A. F. Kip, Phys. Rev. 98, 337 (1955).
[3]R. B. Lewis and T. R. Carver, Phys. Rev. Lett. 12, 693 (1964); and Phys. Rev. 155, 309 (1967).
[4]N. S. Van der Ven and R. T. Schumacher, Phys. Rev. Lett. 12, 695 (1964).
[5]A. Janossy and P. Monod, J. Phys. F 3, 1752 (1973).
[6]L. D. Flesner, D. R. Fredkin, and S. Schultz, Solid State Commun. 18, 207 (1976).
[7]A. Janossy and K. Csermak, Report KFKI-74-17 (Hungarian Acad. Sci., Budapest, 1974).
[8]Richard Magno and Joe H. Pifer, Phys. Rev. B 10, 3727 (1974).
[9]P. Monod, H. Hurdequint, A. Janossy, J. Obert, and J. Chaumont, Phys. Rev. Lett. 29, 1327 (1972).
[10]H. Hurdequint, thesis (University of Paris, Orsay) (unpublished).
[11]M. B. Walker, Can. J. Phys. 52, 2065 (1974).
[12]H. Hasegawa, Prog. Theor. Phys. 21, 483 (1959).
[13]F. Hoffman, thesis (University of Paris, Orsay) (unpublished); and private communication.
[14]A. Janossy and P. Monod, Solid State Commun. 18, 203 (1976).
[15]A. Janossy and J. Kollar, J. Phys. F (to be published).
[16]H. C. Torrey, Phys. Rev. 104, 563 (1956).
[17]M. B. Walker, Phys. Rev. B 3, 30 (1971).
[18]D. R. Fredkin (private communication).
[19]M. R. Menard and M. B. Walker, Can. J. Phys. 52, 61 (1974).